Leukemia (2018) 32:1393–1403
https://doi.org/10.1038/s41375-018-0073-5

ARTICLE

Mechanisms of resistance

# Relapsed acute lymphoblastic leukemia-specific mutations in NT5C2 cluster into hotspots driving intersubunit stimulation

Aleš Hnízda[1,9] · Milan Fábry[2] · Takaya Moriyama[3] · Petr Pachl[1] · Michael Kugler[1,2] · Vítězslav Brinsa[1] · David B. Ascher[4,5] · William L. Carroll[6] · Petr Novák[7] · Markéta Žaliová[8] · Jan Trka[8] · Pavlína Řezáčová[1,2] · Jun J. Yang[3] · Václav Veverka[1]

Received: 5 October 2017 / Revised: 27 January 2018 / Accepted: 1 February 2018 / Published online: 25 February 2018


## Abstract

Activating mutations in NT5C2, a gene encoding cytosolic purine 5′-nucleotidase (cN-II), confer chemoresistance in relapsed acute lymphoblastic leukemia. Here we show that all mutants became independent of allosteric effects of ATP and thus constitutively active. Structural mapping of mutations described in patients demonstrates that 90% of leukemia-specific alleles directly affect two regulatory hotspots within the cN-II molecule—the helix A region: residues 355–365, and the intersubunit interface: helix B (232–242) and flexible interhelical loop L (400–418). Furthermore, analysis of hetero-oligomeric complexes combining wild-type (WT) and mutant subunits showed that the activation is transmitted from the mutated to the WT subunit. This intersubunit interaction forms structural basis of hyperactive NT5C2 in drug-resistant leukemia in which heterozygous NT5C2 mutation gave rise to hetero-tetramer mutant and WT proteins. This enabled us to define criteria to aid the prediction of NT5C2 drug resistance mutations in leukemia.

## Introduction

Relapsed acute lymphoblastic leukemia (ALL) has been shown to be driven by mutations in PRPS1 or NT5C2, genes for enzymes participating in the biosynthetic pathway of purine nucleotides [1–3]. These findings have revealed that the misregulation of metabolic enzymes is a novel mechanism underlying chemoresistance of leukemia cells. Protein oligomerization plays an important role in the functional regulation of many metabolic enzymes [4], and it has been suggested that some of these ALL mutations may act by altering the oligomerization or regulatory sites, inducing constitutive activity [1, 5].

NT5C2 encodes cytosolic purine 5′-nucleotidase (cN-II) which catalyzes dephosphorylation of inosine monophosphate (IMP). This reaction links the de novo synthesis, salvage pathway, and oxidative degradation of purines. Therefore, the cN-II enzyme is strictly regulated, and the presence of adenylate compounds such as ATP is required for full catalytic activity [6]. Allosteric regulation is

**Electronic supplementary material** The online version of this article (https://doi.org/10.1038/s41375-018-0073-5) contains supplementary material, which is available to authorized users.

✉ Aleš Hnízda
ah960@cam.ac.uk

1 Institute of Organic Chemistry and Biochemistry, Academy of Sciences of the Czech Republic, Flemingovo nam. 2, Prague 6 166 10, Czech Republic

2 Institute of Molecular Genetics, Academy of Sciences of the Czech Republic, Videnska 1083, Prague 4 142 20, Czech Republic

3 Department of Pharmaceutical Sciences, St Jude Children's Research Hospital, Memphis, TN, USA

4 Department of Biochemistry, Sanger Building, University of Cambridge, 80 Tennis Court Road, Cambridge CB2 1GA, UK

5 Department of Biochemistry and Molecular Biology, Bio21 Institute, University of Melbourne, 30 Flemington Road, Parkville VIC 3052, Australia

6 NYU Cancer Institute, NYU Langone Medical Center, New York, NY, USA

7 Institute of Microbiology, Academy of Sciences of the Czech Republic, Videnska 1083, Prague 4 142 20, Czech Republic

8 Childhood Leukaemia Investigation Prague, Department of Paediatric Haematology and Oncology, Second Faculty of Medicine, Charles University and University Hospital Motol, Prague, Czech Republic

9 Present address: Department of Biochemistry, University of Cambridge, 80 Tennis Court Road, Cambridge, UK

mediated by the helix A region (residues 355–365), which connects the ATP-binding site and catalytic pocket [7].

We recently showed that the three most common leukemia-specific mutations in NT5C2 lead to significant structural changes in the tetramer interface [5], partly formed by ATP-binding site [7]. The cN-II homotetramer is formed by two identical dimers, mediated by a dimerization site (interface A) which are held together through interaction at interface B [8]. These activating mutations led to complex re-arrangement of these intersubunit contacts, suggesting an important role of the entire oligomeric interface in the allosteric regulation of cN-II activity [5]. However, the structural mechanisms modulating the regulatory network in purine nucleotidase and how other ALL mutations drive resistance is still not well understood, hindering identification of causative variants.

In this study, we uncover the allosteric regulation of the most common cN-II mutants (R367Q and R238W) in more detail using enzymological, structural, and cellular approaches. We also explore structural and biochemical properties of four additional mutations distributed across the cN-II protein (K25E, R39Q, R238G, and S408R). Our work identifies two major mutational hotspots in the cN-II structure establishing a solid framework for assessment of novel genetic variants in NT5C2.

## Materials and methods

### Protein preparations

For structural studies, we prepared C-terminally truncated proteins as described previously [5]. Co-expression of full-length variants was performed using pETDuet-1. Expression and purification is described in Supplementary File.

### X-ray crystallography

Previously, we have determined crystal structures of apo-forms for the most common mutants R367Q and R238W [5]. To determine crystal structures of these variants in the presence of ATP, we prepared them with additional amino acid substitution D52N as described for the wild-type (WT) cN-II [7]. The proteins were crystallized in the presence of 10 mM 2-deoxyadenosine triphosphate (dATP) and 20 mM $MgCl_2$ using sitting drop vapor diffusion technique. Crystallization conditions are specified in Supplementary File. Diffraction data were collected on BL14.1 or BL14.3 operated by the Joint Berlin MX Laboratory at the BESSY II electron storage ring (Berlin-Adlershof, Germany) [9] or at Rigaku HF007. Data processing and refinement is described in Supplementary File. Crystal structures were deposited in the PDB under accession codes: 5OPK (D52N/R367Q+dATP), 5OPM (D52N/R238W+dATP), 5OPN (R39Q), 5OPO (R238G), and 5OPP (S408R), 5OPL (K25E).

### Bioinformatics

To evaluate the structural effects of the mutations on the the WT homotetrameric structures (apo: PDB ID 2XCX; activated PDB ID 2XJD), missing loops were generated using the ModLoop server [10]. The models were then minimized using the MMF94s forcefield in Sybyl-X 2.1.1 (Certara L. P., St Louis, MO). Interactions were calculated and visualized using Arpeggio [11]. The effects of the mutations upon the stability of cN-II were predicted using DUET [12]. The effect of the mutations upon the protein–protein binding affinity of the homotetrameric cN-II assembly were predicted using mCSM-PPI [13].

### Activity assay

Enzyme activity was determined in duplicates of two independent measurements following procedures described previously [5] with 0.2 mM IMP as substrate.

### Mass spectrometry

Presence of both cN-II variants after co-expression was determined using in-gel digestion with trypsin or Asp-N analyzed by mass spectrometry as described previously [14].

### Lentiviral production and NT5C2 overexpression

N-terminal FLAG-tagged NT5C2 cDNAs for R367Q were cloned into the lentiviral vector pLenti. cDNA constructs were transfected into 293T cells along with helper plasmids using the calcium phosphate method to produce replication-defective virus. Supernatant was harvested 48 h later and used to transduce NALM6 and REH human lymphoid cell lines. The cells were grown in RPMI1640 supplemented with 10% fetal bovine serum, 10 mM HEPES and 1 mg/mL Geneticin antibiotic in 5% $CO_2$ at 37 °C. The levels of NT5C2 were determined by immunoblot analysis with anti-FLAG (#2368, Cell Signaling Technology, catalog no. 2368; 1:3000 dilution) antibody, using glyceraldehyde 3-phosphate dehydrogenase as the loading control.

### Cell viability and chemotherapy drug response

NT5C2-overexpressing cells and control cells were treated with thioguanine at the indicated concentrations. After cells had been incubated with the thiopurines for 72 h, the cell viability was assessed at least for three times with triplicates

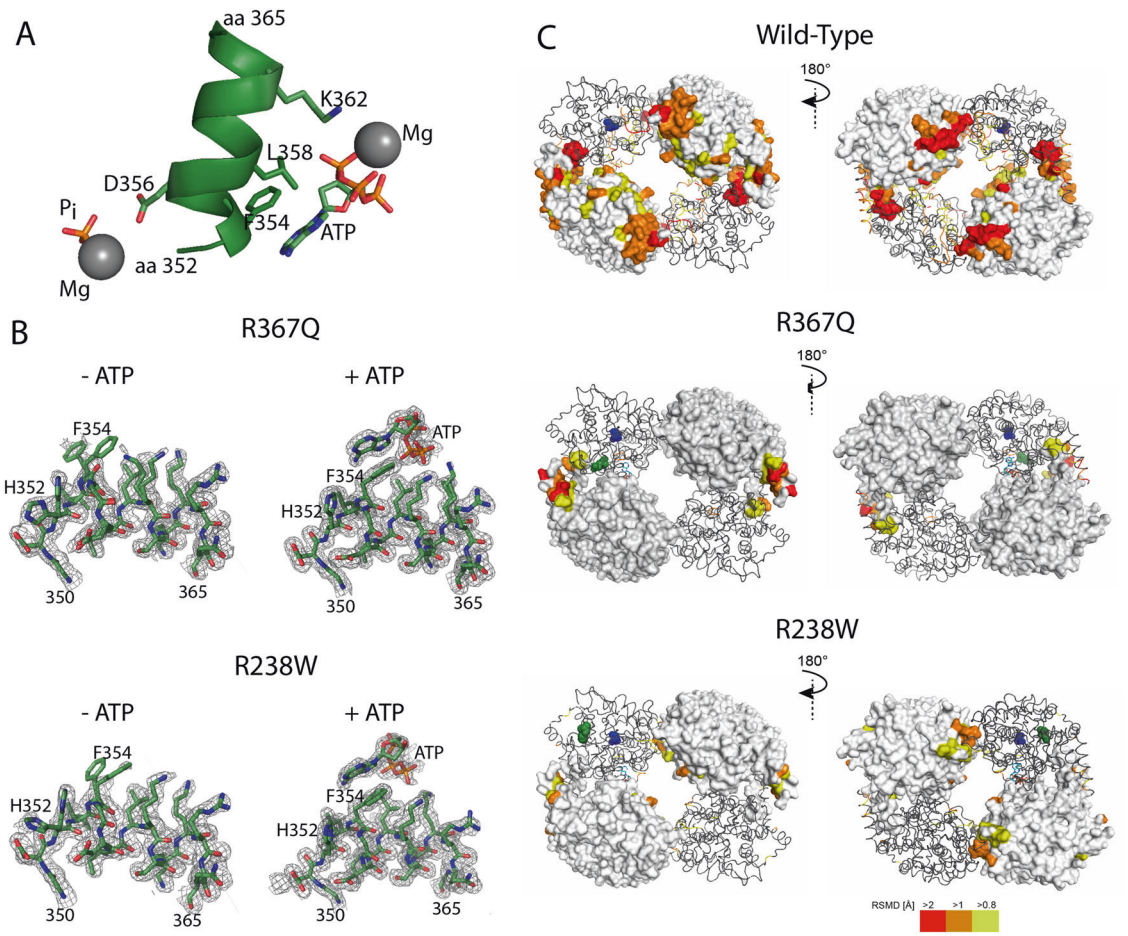


**Fig. 1** Effect of ATP binding on the structure of cN-II mutants R367Q and R238W. **a** Helix A in the structure of the R367Q mutant bound to Mg-ATP (allosteric site) and free phosphate (catalytic pocket). Residues directly involved in the ligand binding, free phosphate, and ATP are highlighted as sticks. Magnesium ions are shown as gray balls. **b** Electron density of the F354 residue illustrates stabilization of this region in the presence of ATP. 2Fo-Fc maps at contour level at 1σ are shown. **c** Global changes in cN-II structure caused by ATP binding in the wild-type and mutants R367Q and R238W. RMSD was calculated using superposition of structures depending on the presence of ATP. The subunits of cN-II tetramer are represented as a light gray surface or dark gray ribbons. The residues with altered position are shaded according to calculated RMSD values (scale bar shown at bottom right). The active site and mutated residues are highlighted as blue and green spheres, respectively, in one of the protein subunits. For this illustration, atom coordinates deposited in Protein Data Bank were used as follows: 2XCX (free WT); 2XCW (WT complexed with ATP); 5K7Y (free R367Q); 5OPK (R367Q complexed with ATP); 5L4Z (free R238W); and 5OPM (R238W complexed with ATP)

using the colorimetric 3-(4,5-dimethylthiazol-2-yl)-2,5-diphenyltetrazolium bromide assay.

## Genetic analysis

In total, 20 out of the 23 children (age 1–18 years) with the bone marrow relapse of BCR/ABL1-negative ALL diagnosed and/or treated in the Czech Republic from August 2013 to January 2017 were analyzed by next-generation sequencing. Bone marrow sample processing and nucleic acid isolations and quality control were performed as described previously [15]. Analysis of DNA from relapse and remission bone marrow samples is described in Supplementary File. Sequencing data were analyzed as described previously [16].

## Statistics

Data are presented as a mean with s.d. Activity measurements and bioinformatics were tested using two tailed Student's *t*-test ($p < 0.05$ and $p < 0.005$, respectively). Cell viability data were evaluated using one-way analysis of variance ($p < 0.001$).

# Results

## cN-II mutants are locked in an active conformation

We recently demonstrated that relapsed leukemia-specific mutations in NT5C2 cause aberrant regulation of cN-II [5].

To better understand altered allosteric motions in the most common mutants (R367Q and R238W), we have determined their structures in the presence of ATP and evaluated conformational changes induced by the activator binding.

We prepared crystals of the mutants complexed with ATP using co-crystallization or soaking experiments. In order to improve quality of the crystals, we introduced an additional D52N mutation and produced double mutants D52N/R367Q and D52N/R238W. As described previously for the WT cN-II, the D52N substitution locks the active site but does not induce additional structural changes across the cN-II tetramer [7]. Therefore, this approach is suitable for obtaining snapshots of cN-II–ligand complexes.

We determined the crystal structures of D52N/R367Q and D52N/R238W in the presence of dATP (Table S1). We observed additional electron density in the ATP-binding and active sites of both mutants, which corresponded to the presence of magnesium ion and phosphate moiety in the catalytic pocket, and to Mg-dATP complex at the binding region for allosteric activators. Similar observations were reported for the WT cN-II [7] (PDB ID 2XJD) consistent with a lack of structural changes within the functional sites of the mutants.

As helix A (residues 355–365) connects the ATP-binding site to the catalytic pocket (Fig. 1a), we looked for ATP-dependent structural changes in this region. In WT cN-II, helix A underwent a disorder-to-order transition upon ATP binding [7]. In contrast, helix A of the mutants was fully structured even in the absence of ATP, with only modest increase in stability when ATP was added which could be observed through slightly better defined electron densities for residues H352 and F354 in the complex with ATP (Fig. 1b). Structural rigidity of helix A has been shown to correlate strongly with cN-II catalytic activity, suggesting that rigidification of helix A plays a crucial role in stimulation of the mutants.

Next, we examined global structural changes induced by ATP binding. While the WT enzyme exhibits extensive changes across the oligomeric interface upon ATP binding (Fig. 1c), structural superposition between the apo and ATP-bound complexes revealed only small differences induced by ATP activator in the mutants (overall root mean square deviation ≈0.3 Å compared with 0.7 Å for the WT). This reveals that ALL-specific mutants predominantly adopt an active conformation even in the absence of physiological activators.

## The effects of mutations are transmitted via intersubunit motions

As hyperactive variants specifically change tetramerization interfaces of cN-II [5], we assessed the stimulatory effects of intersubunit motions induced by mutations. Taking into account heterozygosity of the mutations in relapsed ALL, we examined enzyme activity of hetero-oligomeric complexes consisting of the WT and mutant subunits. Production of cN-II heterotetramers was performed using pETDuet-1 plasmid, a vector allowing co-expression of different variants expressed independently from two T7-promoter-driven transcription units. As a first step, we examined heteromeric WT+R367Q to determine a complementation coefficient (CC) defined as the ratio of measured catalytic activity obtained for heteromeric complex to the arithmetic mean of each component [17]. The heteromeric complex exhibited higher activity than the individual variants, with the CC value of ≈1.5, which strongly demonstrates the positive complementation effect (Table S2).

Subunits in tetrameric proteins are randomly assembled into an array of heteromers having variable composition (subunit ratios of 4:0, 3:1, 2:2, 1:3. 0:4 with the distribution 1:4:6:4:1) [18]. As cN-II protein is not soluble in buffers compatible with native mass spectrometry, we analyzed formation of heteromers using co-expression of two variants bearing different tags (WT-His+R367Q-Strep and WT-Strep+R367Q-His). After nickel affinity chromatography, the co-purification of strep-tag variant was confirmed in both samples using peptide mass fingerprinting, demonstrating the presence of heteromeric cN-II assemblies (Fig. S1). However, strep-tagged cN-II was produced with a lower efficiency than the His-tagged variants, as indicated by the yields for respective affinity purifications (Table S3). Therefore, we could not analyze heteromeric complexes that arose from the equimolar mixtures of protomers.

As an alternative approach, we performed the complementation study of the active and catalytically dead his-tagged variants, which provides a useful tool to explore the propagation of effects of activating mutations across the oligomeric assembly [19]. We introduced the inactivating mutation D52N into one of the two copies of NT5C2 genes expressed by the pETDuet-1 and analyzed five different hetero-oligomeric complexes (Table S4) examining the effect of R367Q and R238W mutations. Peptide mass fingerprinting verified approximately equimolar composition for all co-expressed protein samples (Figures S2–S4).

Examination of the activities for $WT^{active}$+$R367Q^{inactive}$ and $WT^{active}$+$R238W^{inactive}$ heteromeric complexes revealed two-fold higher catalytic potency of both variants, compared to $WT^{active}$+$WT^{inactive}$ (Fig. 2a). This suggested that the effects of activating mutations were transmitted into adjacent subunits, leading to activation of the WT subunit. Next, we looked at $WT^{inactive}$+$R367Q^{active}$ and $WT^{inactive}$+$R238W^{active}$ to examine the activating effects of mutations within the same subunit. The $WT^{inactive}$+$R367Q^{active}$ showed a similar extent of two-fold activation compared to $WT^{active}$+$WT^{inactive}$, demonstrating that the R367Q

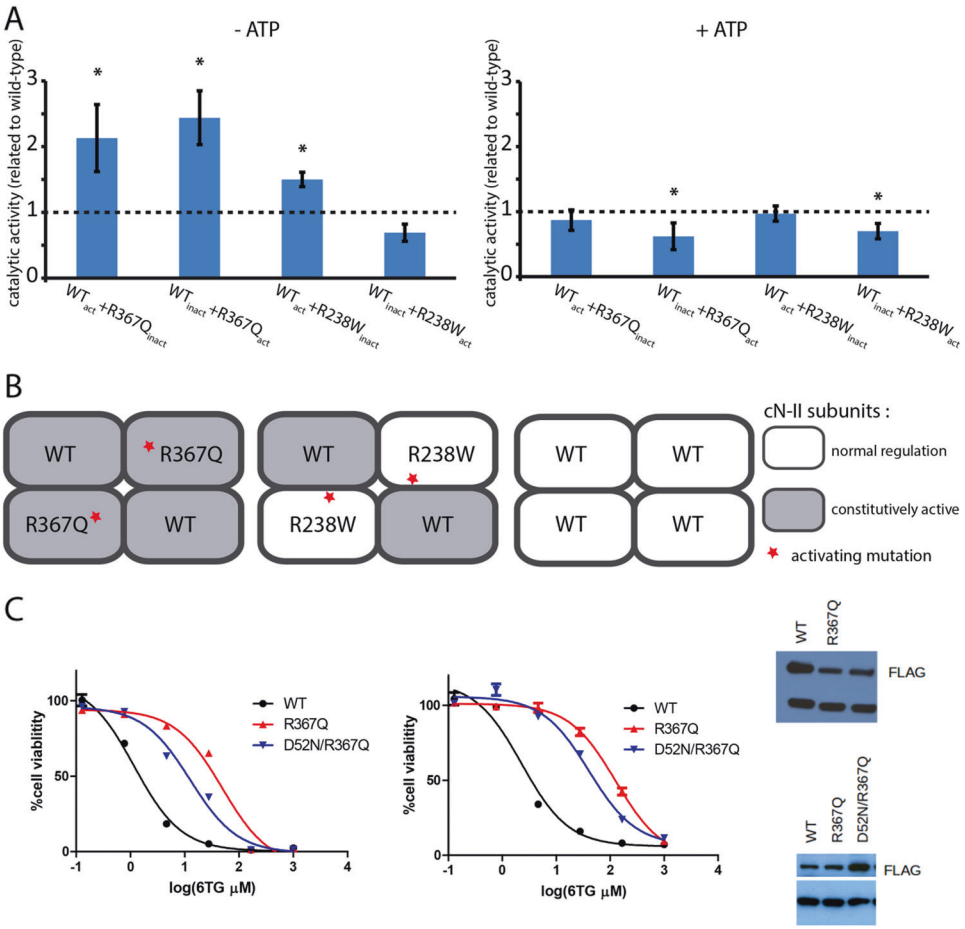


**Fig. 2** Catalytic activity of cN-II hetero-oligomeric complexes depending on the presence of ATP. **a** Relative values compared to the wild-type cN-II are shown. Asterisk means that the value was significantly different from that of wild type as determined by two-tailed Student's *t*-test ($p < 0.05$). **b** Schematic representation of activatory effects for R367Q and R238W mutations. The R367Q activates its own as well as adjacent subunits, while the R238W only the adjacent subunits. Heteromeric complexes may have variable composition (WT–mutant ratio of 4:0, 3:1, 2:2, 1:3, 0:4). For clarity, we present cN-II heteromer having ratio of 2:2 only. **c** Inactive double mutant D52N/R367Q still confers chemoresistance against thioguanine (left and right panels were for Nalm6 and REH, respectively)

mutation led to direct stimulation of the mutated subunit. In contrast, $WT^{inactive}$+$R238W^{active}$ exhibited comparable level of catalytic activity to the $WT^{active}$+$WT^{inactive}$, indicating that the R238W mutation cannot activate the mutant subunit. This demonstrates that the R367Q mutation activates its own as well as adjacent subunit while the R238W acts exclusively through effects on neighboring subunits (Fig. 2b).

To observe intersubunit activation of NT5C2 in leukemic cells, we generated NALM6 and REH cell lines overexpressing WT, R367Q, and the double mutant D52N/R367Q. These recombinant proteins were complemented by endogenously expressed cN-II. We tested whether the inactivating D52N mutation could abolish the chemoresistance conferred by the relapse-specific mutation R367Q. After treating the cells with the chemotherapeutic 6-thioguanine, both the R367Q and the D52N/R367Q mutation showed increased viability of NALM6 cells compared with WT (IC50s were 1.2 ± 1.1, 49.0 ± 1.2, and 12.6 ± 1.2 for WT, R367Q, and D52N/R367Q, respectively) (Fig. 3c). Very similar patterns of resistance were also seen in REH cells (IC50s were 2.3 ± 1.2, 127.0 ± 1.1 and 40.7 ± 1.2 for WT, R367Q, and D52N/R367Q, respectively). These data indicated that the inactivated cN-II carrying R367Q relapse-specific mutation was able to confer chemoresistance in leukemia cells through transmission of activation to the endogenous WT protein.

Taken together, the in vitro and cellular studies demonstrated that mutant and WT subunits assemble into heteromeric complexes in which intersubunit allosteric rearrangement represents an important mechanism for hyperactivation.

## Analysis of three additional mutants demonstrates a common mechanism for hyperactivity

To further explore activating motions in the oligomeric interface of cN-II, we characterized the catalytic properties depending on the presence of ATP for three additional variants identified in relapsed ALL (R39Q, R238G, and S408R). These were compared to the behavior of the WT, our previously described hyperactive mutants (R367Q, R238W, and L375F) and two neutral variants from reference exomes deposited in the EXAC database (T3A and H380R). Basal catalytic activity of leukemic mutants was significantly higher compared to the WT and neutral, but

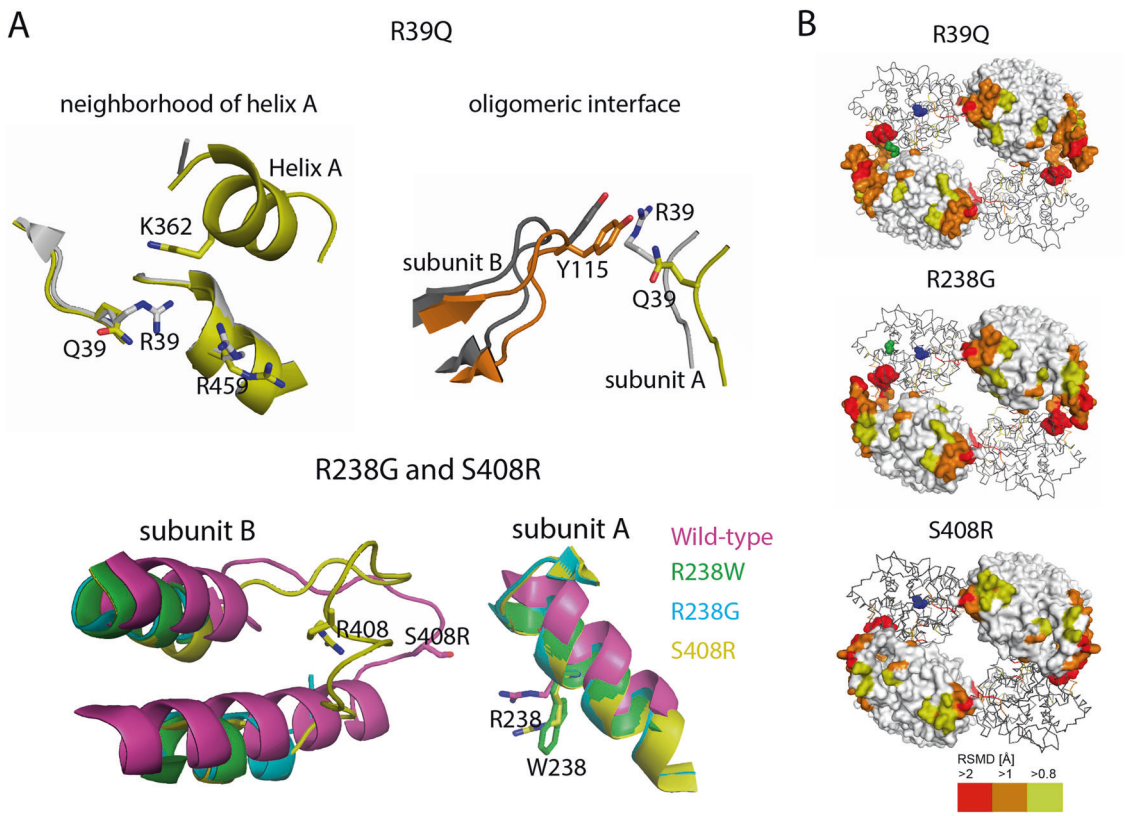


**Fig. 3** Crystal structure of the cN-II mutants R39Q, R238G, and S408R. **a** Local changes induced by leukemia-specific mutations. The R39Q (yellow; PDB ID 5OPN) is compared with wild type (white; PDB ID 2XCX), the second subunit is highlighted in orange (R39Q) or gray (wild type). The R238G (cyan; PDB ID 5OPO) and S408R (yellow; PDB ID 5OPP) are shown together with wild type (magenta) and R238W (green; PDB ID 5L4Z). A loop between helixes, not found in the crystal structure, was modeled using the ModLoop server and shown only for S408R and wild type. **b** Global structural changes revealed by superposition of the mutants (R39Q, R238G, and S408R) with wild type. The subunits of cN-II tetramer are represented as a light gray surface or dark gray ribbons. The residues with altered position are shaded according to calculated RMSD values (scale bar shown at bottom right). The active site and mutated residues are highlighted as blue and green spheres, respectively, in one of the protein subunits

this relative difference was almost abolished in the presence of 3 mM ATP (Table 1). This showed that the increased basal activity of the mutants represents an important biochemical measure for the pathogenicity of cN-II variants.

To complement enzyme activity measurements, we examined in detail crystal structures of the leukemia-specific mutants R39Q, R238G, and S408R (Table S1). We probed both the local and global changes induced by the respective mutations.

The R39Q mutation lies at loop 34–42 connecting two 3/10 helixes in close proximity to helix A (Fig. 3a). R39 makes a number of key intramolecular and intermolecular polar and pi interactions, which cannot all be maintained upon mutation to glutamine, including interaction to the backbone carbonyls of residues M455, R456, and A485 and side chains of D459 and Y115. Because the segment 455–459 plays an important role in the rearrangement of helix A during the stimulation of cN-II upon ATP binding, the altered interactions here help to induce the stimulatory motions within the enzyme. Moreover, the R39Q mutation results in the re-orientation of the Y115 side-chain from the adjacent subunit, displacing by 0.2 Å away from the oligomeric interface. The R39Q variant thus stimulates cN-II

**Table 1** Catalytic activity of the cN-II mutants

| | Activity (μmol/min/mg) | |
|---|---|---|
| 3 mM ATP | − | + |
| Wild type | 0.27 ± 0.03 | 6.51 ± 0.88 |
| T3A | 0.22 ± 0.03 | 6.7 ± 1.4 |
| H380R | 0.25 ± 0.03 | 4.23 ± 0.69[a] |
| R367Q | 0.70 ± 0.09[a] | 7.4 ± 4.1 |
| R238W | 0.41 ± 0.04[a] | 5.09 ± 0.85 |
| L375F | 0.63 ± 0.14[a] | 8.50 ± 0.91 |
| R39Q | 1.23 ± 0.14[a] | 13.4 ± 6.8 |
| R238G | 0.68 ± 0.11[a] | 12.8 ± 1.4[a] |
| S408R | 0.54 ± 0.12[a] | 7.2 ± 0.81 |

Measurements were performed with 0.2 mM IMP

[a] Value was significantly different from that of wild type ($p < 0.05$)

**Table 2** List of NT5C2 mutations identified in relapsed ALL and their structural positions

| Mutation | Number of patients | Reference | Structural location | Change in stability (active–inactive state) (kcal/mol) |
|---|---|---|---|---|
| R367Q | 31 | [2, 3, 21–24][a] | Hotspot 1 | 0.215 |
| R238W | 13 | [2, 3, 21, 23] [a] | Hotspot 2 | 0.353 |
| S408R | 2 | [3, 21] | Hotspot 2 | 0.516 |
| L375F | 3 | [2, 23] | Area interacting with C-terminus | 0.054 |
| R39Q | 4 | [21, 23][a] | Hotspot 1 | 0.067 |
| R238G | 3 | [21, 23] | Hotspot 2 | 0.209 |
| R238Q | 1 | [21] | Hotspot 2 | 0.269 |
| S360P | 1 | [21] | Hotspot 1 | 0.308 |
| R238L | 1 | [2] | Hotspot 2 | 0.192 |
| R291W | 1 | [2] | Oligomeric interface B—substrate channel | 0.685 |
| K359Q | 1 | [2] | Hotspot 1 | 0.2 |
| K404ins | 1 | [3] | Hotspot 2 | NA |
| D407A | 1 | [2] | Hotspot 2 | 1.136 |
| D407Y | 2 | [23, 24] | Hotspot 2 | 1.177 |
| P414S | 2 | [23, 24] | Hotspot 2 | 0.324 |
| S445F | 1 | [3] | Area interacting with C-terminus | 0.076 |
| Q523[a] | 1 | [2] | Area interacting with C-terminus | NA |
| del 397-399 | 1 | [24] | Hotspot 2 | NA |
| T489M | 1 | [21] | Area interacting with C-terminus | 0.154 |
| D407H | 1 | [21] | Hotspot 2 | 1.34 |
| R195Q | 1 | [21] | Oligomeric interface B—substrate channel | 0.35 |
| R34Q | 1 | [21] | Area interacting with C-terminus | −0.134 |
| P533L | 1 | [21] | Area interacting with C-terminus | 0.315 |
| K25E | 1 | [a] | Hotspot 2 | 0.057 |
| D407V | 1 | [23] | Hotspot 2 | 0.234 |

Hotspot #1 and #2 refers to helix A and its proximity and to interaction area between regions helix B and loop L, respectively

[a] Mutations from our current study

activity via direct changes in the proximity of the helix A as well as structural modulation of the oligomeric interface.

Several somatic mutations cause a replacement of the R238 residue (R238W, R238G, R238Q, and R238L), which is localized at α-helical region 232–242 (helix B). The structural effects of R238W have been described previously [5], and in this work, we analyzed the R238G mutant. Comparison of the R238W and R238G structures revealed very similar local effects of the mutations (Fig. 3a) indicating a common mode of action for both mutations. The R238 side-chain of the WT is oriented toward the adjacent subunit and may interact with interhelical loop 400–418 (loop L). While loop L is not assigned in most crystal structures of cN-II due to high flexibility, snapshots of interacting residues have been revealed by loop modeling in the WT cN-II [5] and were recently captured in an experimental structure with a noncompetitive inhibitor [20]. In particular, intersubunit contacts between R238 and S408 were found in the inactive state of cN-II (PDB ID 5CQZ). Therefore, replacement of positively charged R238 probably decreases the tendency to form these transient polar contacts with the flexible loop at the oligomeric interface, which in turn induces activation of the enzyme.

Interestingly, several mutations are also localized in loop L, in particular D407A, D407H, D407Y, D407V, S408R, and P414S. As a representative variant perturbing this

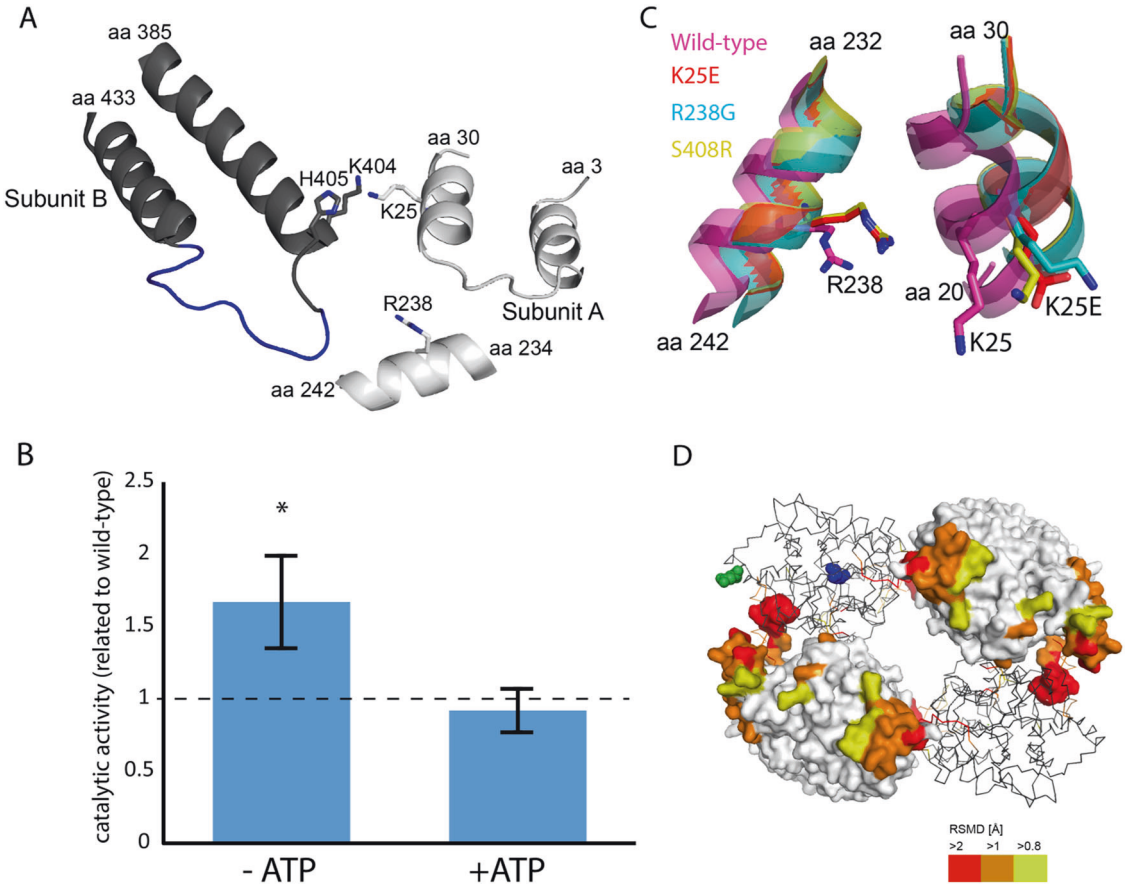


**Fig. 4** Characterization of novel relapsed ALL-specific variant K25E. **a** The K25 residue and its positioning in respect of hotspot area consisting of regions 232–242 and 400–418. Structure of wild-type cN-II (PDB ID 2XCX) is used for illustration. Loop highlighted in blue is not present in the crystal structure and was built using the ModLoop server. **b** Examination of catalytic activity in the presence and absence of ATP. Relative values compared to the wild-type cN-II are shown. Asterisk means that the value was significantly different from that of wild type as determined by two-tailed Student's *t*-test ($p < 0.05$). **c** Structural topology of residues 25 and 238 in the K25E (red), wild type (magenta), and two other hyperactive mutants (R238G in cyan and S408R in yellow). **d** Global structural changes induced by K25E mutation (PDB ID 5OPL) as revealed by structural superposition of K25E mutants with the wild-type cN-II. The subunits of cN-II tetramer are represented as a light gray surface or dark gray ribbons. The residues with altered position are shaded according to calculated RMSD values (scale bar shown at bottom right). The active site and mutated residues are highlighted as blue and green spheres, respectively, in one of the protein subunits

region, the S408R mutant was characterized. In agreement with the structural data described above, the S408R mutation caused displacement of the R238 residue from an adjacent subunit (Fig. 3a), indicating that local effects of S408R were highly similar to the mutations at the 238 position. This suggests that contact area between helix B and loop L represents a mutational hotspot in cN-II leading to activation.

To assess global structural changes of the studied mutations, structural superposition with the WT cN-II (PDB ID 2XCX) revealed significant conformational changes at the oligomeric interfaces, as we observed previously for three different mutations [5] (Fig. 3b). This strongly supports a shared mechanism for NT5C2-activating mutations acting through specific changes at oligomerization sites. In summary, structural data from the extended set of hyperactive mutations strongly demonstrate that the oligomeric interface represents a key region for cN-II activation.

## ALL-specific mutations destabilize inactive conformation of cN-II protein

To further explore shared structural changes in leukemic NT5C2 variants, we analyzed the effects of mutations on stability of the cN-II conformers represented by crystal structures for inactive and active form of WT cN-II. Interestingly, the ALL-specific cN-II mutations were located significantly closer to the homotetramer interfaces in the inactive, but not the activated, conformation than the 10 most common missense variants from EXAC (Table S5). This suggested that the ALL-specific variants could

more significantly affect the formation of the inactivated homotetramer than the activated conformation. To test this notion, we applied established bioinformatic tools, in particular DUET [12] and mCSM-PPI [13], which revealed that vast majority (21 of the 22) of the ALL-specific variants destabilized the inactive conformation of cN-II significantly more than the activated form, leading to a shift in conformational equilibrium towards the activated conformation (Table 2). This supports the notion that all relapse-specific mutations act through shared structural mechanism and provide a measure to assess novel variants.

### Novel mutation K25E expands a set of characterized cN-II variants

Finally, we utilized the previously acquired structural knowledge to assess novel NT5C2 variants in relapsed ALL. We identified three patients experiencing relapsed B-cell precursor ALL with mutations in NT5C2. In two patients, we found variants that have already been examined (#1—R367Q and R238W, variant allele frequencies 17% for both; #2—R39Q, variant allele frequency 40%). Interestingly, leukemic cells of patient #3 carried a novel variant K25E (variant allele frequency 40%). RNA-seq showed that all mutated alleles were expressed in leukemic cells.

The K25E mutation lies close to the hotspot area making intersubunit contacts between helix B and loop L (Fig. 4a) and was predicted by mCSM-PPI and DUET to increase stability of activated conformation relative to the inactive form, leading to enzyme hyperactivity. To test this prediction, we analyzed catalytic and structural properties of the K25E mutant.

We compared the enzyme activity of the K25E with the WT cN-II depending on the presence of ATP. In the absence of ATP activator, the K25E mutant exhibited significantly higher catalytic activity than WT while no significant changes were found in the presence of 3 mM ATP (Fig. 4b). Similar observation was made for the other leukemia-specific variants tested previously. Furthermore, analysis of the crystal structure showed similar changes as those observed for other mutations located in the same region (R238W, R238G, and S408R). In particular, residues E25 and R238 were displaced from the oligomerization interface, inducing distant structural changes including rearrangement of tetramerization sites and stabilization of helix A (Fig. 4c, d). Taken together, activity measurements coupled with structural analysis confirmed functional effects of novel leukemia-specific variant. We demonstrate here that detailed structural data provide useful framework for evaluation of novel disease-causing variants in the NT5C2 gene.

## Discussion

Hyperactivity of cN-II represents an important mechanism for driving relapsed ALL. Our previous structural studies on the most common mutants revealed that the hyperactivity is caused by altered allosteric regulation due to conformational changes at the oligomerization interfaces of the cN-II tetramer. However, allosteric motions along proteins are very complex and can be difficult to predict. Here we investigated the impaired regulation of cN-II on an extended set of mutants representing major hotspots within the protein structure.

To our knowledge, 25 different mutations in NT5C2 have been described in relapsed ALL [2, 3, 21–24] and all of them are localized at the oligomeric interfaces of cN-II (Table 2). According to their position within the three-dimensional structure of cN-II, we can clearly recognize that cN-II contains two hotspots (Fig. 5): helix A and its neighborhood (50% cases) and intersubunit contact area between helix B and loop L (40% cases).

Variants in helix A region, which undergoes disorder–order transition required for full activity of cN-II [7], lead to stabilization of the ordered state. While there is less structural information available for the second hotspot between helix B and loop L, recent structural data suggest that the interaction between these regions is only formed in the inactive state of cN-II and that ALL-associated variants lead to disruption of this interaction. Interestingly, the most frequent mutations in this site are likely to destabilize the intersubunit contacts through changes in side-chain charge (R238W, R238G, S408R, and D407Y).

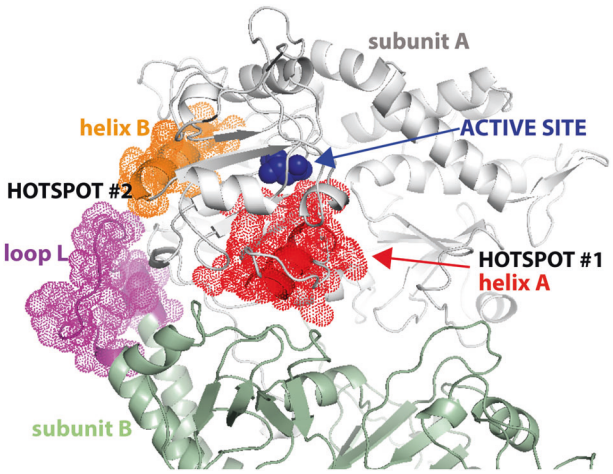


**Fig. 5** Mutational hotspots in cN-II structure. Hotspot #1 (highlighted in red) is formed by helix A area (50% patients) and hotspot #2 (orange and purple) is formed by the interface between helix B and loop L (40% patients). Only one active site (blue spheres) out of four present in the tetramer is shown for clarity. Subunits are represented in different colour (gray and green)

Genetic studies revealed that somatic mutations in NT5C2 are heterozygous and cancer cells produce hetero-tetrameric complexes combining both WT and mutant subunits. We show here that the ALL-specific variants can lead to significant stimulation of the WT subunits, leading to cellular chemotherapeutic resistance. This phenomenon of interallellic complementation has been implicated in adenylosuccinate lyase deficiency or cancer-specific mutations in isocitrate dehydrogenase [17, 25]. Interestingly, while the R367Q acted through both the intersubunit and intrasubunit movements, R238W only led to intersubunit activation. This strongly agrees with the location of the mutations, as R238W lies at the oligomeric interface but far away from helix A, while R367Q is localized in close proximity. This highlights that interallelic effects are of great importance for molecular pathology of NT5C2 gene. Our findings implicate that heterozygous mutations give rise to heteromeric complexes of unique behavior that significantly differs from the homotetramers composed exclusively from individual variants. However, our efforts to purify and characterize particular heteromers were unsuccessful. Of note, rapid progress in single-particle cryo-electron microscopy opens a new opportunity for future studies of cN-II oligomers [26].

While the role of mutations in NT5C2 in chemoresistant leukemia has been previously described [2, 3], the underlying biological mechanisms are poorly understood. It has been hypothesized that cN-II is involved in metabolism of thiopurines [27], which have been used during treatment of ALL for several decades. Recent paper reported that activating mutations are associated with increased export of endogenous purines into extracellular space [28], which in turn might provide selective advantage to all of the leukemic cells in the microenvironment, even to the subclones without NT5C2 mutations.

However, a search of the COSMIC database found a significant number of mutations in NT5C2 in various cancer types, including ones that are not subjected to thiopurine-based treatment. Many of them likely lead to misregulation of cN-II, therefore suggesting that they may have some selective advantage beyond resistance to thiopurine. Interestingly, a recent work has shown that cN-II regulates cellular response to glucose deprivation [29]. Future studies should investigate distant metabolic changes caused by NT5C2 mutations that might uncover general biological mechanisms underlying chemoresistant leukemia.

In summary, this study provides comprehensive molecular insights into activating mutations in NT5C2. Data presented here serve as a framework for assessing the significance of novel variants as demonstrated by the analysis of ALL-specific mutation and by in silico searches through genetic databases.

**Acknowledgements** This work was supported by grant 15-06582S from the Czech Science Foundation and in part by the Ministry of Education of the Czech Republic (program "NPU I" LO1304 and program "InterBioMed" LO1302) and by European Regional Development Fund Project No. CZ.02.1.01/0.0/0.0/16_019/0000729. Institutional support was provided by projects RVO 61388963 and 68378050 of the Academy of Sciences of the Czech Republic. MZ and JT were funded by grant 15-30626A from Czech Health Research Council and grant Primus/MED/28 from Charles University. DBA was supported by a C. J. Martin Research Fellowship from the National Health and Medical Research Council of Australia (APP1072476) and the Jack Brockhoff Foundation (JBF 4186, 2016). We acknowledge beamline access at MX14.1 and MX14.3 of the BESSY (HZB Berlin, Germany) to collect crystal diffraction data. The authors would like to thank Irena Sieglova, MSc and Anna Soldanova, BSc for technical help during protein preparations and Katsiaryna Tratsiak, MSc for crystallization trials.

## Compliance with ethical standards

**Conflict of interest** The authors declare that they have no conflict of interest.

## References

1. Li BS, Li H, Bai Y, Kirschner-Schwabe R, Yang JJ, Chen Y, et al. Negative feedback-defective PRPS1 mutants drive thiopurine resistance in relapsed childhood ALL. Nat Med. 2015;21:563–71.
2. Tzoneva G, Perez-Garcia A, Carpenter Z, Khiabanian H, Tosello V, Allegretta M, et al. Activating mutations in the NT5C2 nucleotidase gene drive chemotherapy resistance in relapsed ALL. Nat Med. 2013;19:368–71.
3. Meyer JA, Wang J, Hogan LE, Yang JJ, Dandekar S, Patel JP, et al. Relapse-specific mutations in NT5C2 in childhood acute lymphoblastic leukemia. Nat Genet. 2013;45:290–4.
4. Fatmi MQ, Chang CE. The role of oligomerization and cooperative regulation in protein function: the case of tryptophan synthase. PLoS Comput Biol. 2010;6:e1000994.
5. Hnizda A, Skerlova J, Fabry M, Pachl P, Sinalova M, Vrzal L, et al. Oligomeric interface modulation causes misregulation of purine 5 -nucleotidase in relapsed leukemia. BMC Biol. 2016;14:91.
6. Spychala J, Madrid-Marina V, Fox IH. High Km soluble 5'-nucleotidase from human placenta. Properties and allosteric regulation by IMP and ATP. J Biol Chem. 1988;263:18759–65.
7. Wallden K, Nordlund P. Structural basis for the allosteric regulation and substrate recognition of human cytosolic 5'-nucleotidase II. J Mol Biol. 2011;408:684–96.
8. Wallden K, Stenmark P, Nyman T, Flodin S, Graslund S, Loppnau P, et al. Crystal structure of human cytosolic 5'-nucleotidase II: insights into allosteric regulation and substrate recognition. J Biol Chem. 2007;282:17828–36.
9. Mueller U, Darowski N, Fuchs MR, Forster R, Hellmig M, Paithankar KS, et al. Facilities for macromolecular crystallography at the Helmholtz-Zentrum Berlin. J Synchrotron Radiat. 2012;19:442–9.
10. Fiser A, Sali A. ModLoop: automated modeling of loops in protein structures. Bioinformatics. 2003;19:2500–1.
11. Jubb HC, Higueruelo AP, Ochoa-Montano B, Pitt WR, Ascher DB, Blundell TL. Arpeggio: a web server for calculating and visualising interatomic interactions in protein structures. J Mol Biol. 2017;429:365–71.
12. Pires DE, Ascher DB, Blundell TL. DUET: a server for predicting effects of mutations on protein stability using an integrated

computational approach. Nucleic Acids Res. 2014;42(Web Server issue):W314–319.
13. Pires DE, Ascher DB, Blundell TL. mCSM: predicting the effects of mutations in proteins using graph-based signatures. Bioinformatics. 2014;30:335–42.
14. Rozbesky D, Sovova Z, Marcoux J, Man P, Ettrich R, Robinson CV, et al. Structural model of lymphocyte receptor NKR-P1C revealed by mass spectrometry and molecular modeling. Anal Chem. 2013;85:1597–604.
15. Zaliova M, Kotrova M, Bresolin S, Stuchly J, Stary J, Hrusak O, et al. ETV6/RUNX1-like acute lymphoblastic leukemia: a novel B-cell precursor leukemia subtype associated with the CD27/CD44 immunophenotype. Genes Chromosomes Cancer. 2017;56:608–16.
16. Kotrova M, Musilova A, Stuchly J, Fiser K, Starkova J, Mejstrikova E, et al. Distinct bilineal leukemia immunophenotypes are not genetically determined. Blood. 2016;128:2263–6.
17. Zikanova M, Skopova V, Hnizda A, Krijt J, Kmoch S. Biochemical and structural analysis of 14 mutant adsl enzyme complexes and correlation to phenotypic heterogeneity of adenylosuccinate lyase deficiency. Hum Mutat. 2010;31:445–55.
18. Yu B, Howell PL. Intragenic complementation and the structure and function of argininosuccinate lyase. Cell Mol Life Sci. 2000;57:1637–51.
19. Baker RP, Urban S. Cytosolic extensions directly regulate a rhomboid protease by modulating substrate gating. Nature. 2015;523:101–5.
20. Marton Z, Guillon R, Krimm I, Preeti, Rahimova R, Egron D, et al. Identification of noncompetitive inhibitors of cytosolic 5 '-nucleotidase II using a fragment-based approach. J Med Chem. 2015;58:9680–96.
21. Ma X, Edmonson M, Yergeau D, Muzny DM, Hampton OA, Rusch M, et al. Rise and fall of subclones from diagnosis to relapse in pediatric B-acute lymphoblastic leukaemia. Nat Commun. 2015;6:6604.
22. Kunz JB, Rausch T, Bandapalli OR, Eilers J, Pechanska P, Schuessele S, et al. Pediatric T-cell lymphoblastic leukemia evolves into relapse by clonal selection, acquisition of mutations and promoter hypomethylation. Haematologica. 2015;100:1442–50.
23. Richter-Pechanska P, Kunz JB, Hof J, Zimmermann M, Rausch T, Bandapalli OR, et al. Identification of a genetically defined ultra-high-risk group in relapsed pediatric T-lymphoblastic leukemia. Blood Cancer J. 2017;7:e523.
24. Ding LW, Sun QY, Mayakonda A, Tan KT, Chien W, Lin DC, et al. Mutational profiling of acute lymphoblastic leukemia with testicular relapse. J Hematol Oncol. 2017;10:65.
25. Reitman ZJ, Yan H. Isocitrate dehydrogenase 1 and 2 mutations in cancer: alterations at a crossroads of cellular metabolism. J Natl Cancer Inst. 2010;102:932–41.
26. Doerr A. Single-particle cryo-electron microscopy. Nat Methods. 2016;13:23.
27. Aster JC, DeAngelo DJ. Resistance revealed in acute lymphoblastic leukemia. Nat Med. 2013;19:264–5.
28. Tzoneva G, Dieck CL, Oshima K, Ambesi-Impiombato A, Sanchez-Martin M, Madubata CJ, et al. Clonal evolution mechanisms in NT5C2 mutant-relapsed acute lymphoblastic leukaemia. Nature. 2018;553:511–4.
29. Bricard G, Cadassou O, Cassagnes LE, Cros-Perrial E, Payen-Gay L, Puy JY, et al. The cytosolic 5'-nucleotidase cN-II lowers the adaptability to glucose deprivation in human breast cancer cells. Oncotarget. 2017;8:67380–93.